Journal of Applied Polymer Science

Fabrication and Characterization of Sucrose Palmitate Reinforced Poly(lactic acid) Bionanocomposite Films

Ravi Babu Valapa, G. Pugazhenthi, Vimal Katiyar
Department of Chemical Engineering, Indian Institute of Technology Guwahati, Guwahati-781039, Assam, India
Correspondence to: V. Katiyar (E-mail: vkatiyar@iitg.ernet.in) and G. Pugazhenthi (pugal@iitg.ernet.in)

ABSTRACT: Environmental issues concerning petroleum-based polymers have begun a growing emphasis to utilize sustainable poly(lactic acid) (PLA) based packaging. However, PLA has its own limitations such as brittleness, high gas permeabilities and slow crystallization rate. With the aim to alleviate these limitations, we made a maiden effort to use a food additive, sucrose palmitate (SP) as eco-friendly filler for fabrication of PLA based bionanocomposites. FTIR analysis elucidated the presence of hydrogen bonding and intermolecular interaction between PLA and reinforcement. Ordered orientation of the SP in the PLA matrix visualized by TEM analysis revealed uniform dispersion of SP filler into PLA matrix. DSC and XRD results confirmed that the incorporated bio-filler acted as a nucleating agent and thus partially contributed towards the crystallinity of PLA-SP bionanocomposites. Enhancement in the tensile strength and elongation at break up to 83 and 56% respectively is obtained. The best positive influence for the oxygen barrier was confirmed for the PLA-SP bionanocomposite film where the reduction in oxygen permeability by 69% is achieved in comparison to pure PLA. © 2014 Wiley Periodicals, Inc. J. Appl. Polym. Sci. **2015**, *132*, 41320.

KEYWORDS: biodegradable; biopolymers and renewable polymers; composites; packaging

Received 6 March 2014; accepted 22 July 2014
DOI: 10.1002/app.41320

INTRODUCTION

Polymer based packaging plays an important role in the modern society, as it is not only providing ease in handling, storage efficiency, attractiveness, light weight, inexpensiveness, and prolong product display but also possibly protecting food from spoilage by microbial contamination, physical damage or bio-chemical reactions during storage.[1–3] Although, plastics serve as one of the cheapest sources available for food packaging, their fossil fuel origin and long-term impact on the environment have spurred research in recent years on search for degradable packaging plastics.[4]

Biopolymers derived from renewable resources can be powerful replacements for conventional plastic packaging materials due to superior degradability and eco-friendly nature.[5] To compete with petroleum-based products, economically suited biodegradable materials which can be easily molded into different forms become a prerequisite factor. Poly(lactic acid) (PLA) is one of such potential representative biodegradable polymers, which has rapidly become the most industrialized bio-sourced synthetic polyester. PLA is a linear, aliphatic, thermoplastic polyester that can be produced from either L-lactic acid or D-lactic acid monomers for useful applications. These monomers are obtained through fermentation of corn starch, sugarcane juice or other agricultural resources.[6,7] PLA is commercially available in variety of grades[8–10] and has been approved by the U.S. Food and Drug Administration (FDA).[8–10] Although PLA exhibits enormous applications in packaging, its intrinsic mechanical property, low crystallization rate and barrier effects to gaseous substances, such as water vapor, oxygen (O_2), carbon dioxide (CO_2) and organic volatiles limit its versatility as food packaging material.[11–13] Although the tensile strength of PLA is almost comparable with the conventional plastics like polyethylene terephthalate (PET), ductility should be improved for PLA. It is indeed necessary to improve the crystallization rate of PLA. This is because, the perfect crystallization in the crystalline area accounts for the compact arrangement of molecular chains which in turn improves mechanical properties and mean while enhances the barrier properties.[14]

Till date, many strategies have been reported to tune PLA properties as a function of chemical structure, structural morphology and its compatibility with other fillers.[15] These include: (i) polymer blending with organic and inorganic fillers[15] and (ii) addition of plasticizer.[4,16–18] Over the past few years, the incorporation of nano-sized bio-fillers in PLA matrix to produce bionanocomposite materials has been explored as an innovative and effective alternative over the traditional technologies for enhancing the mechanical performance, thermal stability and barrier properties of PLA.[4,17,18] At the

nanoscale, such particles have significantly large surface area and exhibit the possibility to interfere with polymer chain mobility, thereby manipulating the matrix properties.[19–22] Hence, it is important to understand that the expected improvements are directly dependent on the dispersion of the nanoparticles in the polymer matrix which manipulate physical or chemical interaction between the matrix and the reinforcing phases. The optimization of dispersion and interactions of nanoparticles in polymer matrices through mechanical and chemical approaches plays a key role for the development of high quality bionanocomposites.

Numerous studies involving a variety of fillers in the development of PLA based bionanocomposites have endeavored.[5,15,17,18] More recently, graphene,[23] silica nanoparticles,[24] carbon nanotubes,[25] and other inorganics[19] are increasingly used as load-bearing constituents in developing PLA composites due to their high aspect ratio and good mechanical properties.[23–26] Enhancement in the tensile strength due to high aspect ratio of the filler (~53 MPa for PLA and ~60 MPa for PLA-CNT composites) was reported using melt compounding by Park et al.[22] Yan and coworkers incorporated silica nanoparticles in the PLA matrix using solution casting method and improvement in the tensile strength (~15.5 MPa for PLA and ~17.5 MPa for PLA-silica composites) was observed due to good compatibility and interfacial combination strength between the filler and PLA matrix.[21] Especially for food packaging applications, it is important to understand not only the physical and mechanical properties of filler materials, but also their compatibility with food during storage becomes a foremost prerequisite factor.[27] Hence, exploration of nontoxic substances approved for food contact needs to be prospected as fillers. Few attempts were made to produce PLA composite systems based on bio-fillers that are nontoxic in nature.[28–37] The effect of different bio-fillers such as starch,[28] olive pit powder,[29] limonene,[30] chitosan,[31] cellulose nanocrystals,[32] kenaf fibers,[33] talc,[34] soy protein,[35] jute fibers,[36] cellulose actetate butyrate[37] on the thermal, mechanical, and gas barrier properties of PLA are investigated. In this study, we have chosen U.S FDA approved food additive, sucrose palmitate (SP) as eco-friendly filler for fabrication of PLA bionanocomposites.[26] Sucrose esters (SEs) are nonionic in nature that are characterized by the presence of hydrophilic and hydrophobic moieties, provided by sugar (sucrose) and alkyl chain (ester), respectively.[26] Besides, SEs being readily biodegradable and nontoxic, they exhibit antimicrobial, mechanical and barrier properties, which make them potential for the storage of food.[26] In the study described here, PLA-SP based bionanocomposites film processing is investigated. Here, the influence of the bio-filler on morphological, thermal, mechanical and barrier properties of PLA composites are examined.

EXPERIMENTAL

Materials

SP manufactured by Sisterna (Netherlands) was used as a filler material. PLA grade 2003D obtained from Nature Works® (USA) was used as a polymer matrix. Chloroform obtained from Merck (India) was used as the solvent for fabrication of PLA-SP bionanocomposites films.

Nanocomposite Preparation

PLA-SP composites were fabricated by solution-casting method as follows: ~0.95 g of PLA was mixed in 50 mL of chloroform and subsequently the mixture was stirred for 2 h in order to completely dissolve the PLA. Likewise above, various concentrations of SP (1, 3, 5, 10, 15, 30 wt % with respect to PLA) was dispersed in chloroform with continuous stirring for 1 h. Subsequently, this solution containing dispersed SP was transferred into PLA-chloroform mixture under vigorous stirring. PLA-SP solution was casted on teflon petriplates and further dried under ambient condition for 24 h. The dried composite films were peeled off carefully from the petriplates. The resulting films were finally oven dried under vacuum for 12 h at 40°C and stored in airtight bags at room temperature for further characterizations. All the samples are designated as SP, PLA, PLA-SP-1, PLA-SP-3, PLA-SP-5, PLA-SP-10, PLA-SP-15, and PLA-SP-30 for SP, PLA, PLA/SP 1 (wt %), PLA/SP 3 (wt %), PLA/SP 5 (wt %), PLA/SP 10 (wt %), PLA/SP 15 (wt %), and PLA/SP 30 (wt %), respectively. The thickness of the fabricated films was measured using film thickness meter (Indi 1652). Twenty measurements were taken on each film and the average thickness of the films is found to be 60 ± 5 μm.

Characterization

Thermogravimetric Analysis (TGA). Thermogravimetric analysis was performed on a Mettler Toledo thermo gravimetric analyzer (TGA/SDTA 851® model). Samples (10.5 ± 0.3 mg) were placed in 900 μL crucible. Pure PLA and PLA-SP bionanocomposites were heated from 25 to 700°C in a 60 mL/min flow of N_2 at a heating rate of 20°C/min.

Differential Scanning Calorimetry (DSC). Thermal properties and crystallization behavior of PLA and PLA-SP bionanocomposites were studied using a differential scanning calorimeter (Mettler Toledo-1 series). Samples (10 ± 0.5 mg) were hermetically sealed in aluminum pans and heated from 25 to 180°C at a heating rate of 5°C/min in an inert atmosphere (N_2 flow, 50 mL/min). All the samples were first heated from 25 to 180°C and held at this temperature for 5 min to eliminate the effect of the thermal and processing history. Glass transition temperature (T_g), cold crystallization temperature (T_{cc}), the enthalpy change at T_{cc} (ΔH_{cc}), melting temperature (T_m) and the enthalpy of fusion at T_m (ΔH_m) of pure PLA and bionanocomposites films were determined from the DSC thermograph during second heating cycle. The T_g was obtained from the midpoint of heat changes from the DSC curves. The percentage crystallinity (% X_c) of PLA was calculated according to the fallowing relation.[27]

$$\%X_c = \frac{(\Delta H_m - \Delta H_{cc})}{(\Delta H_{mp})} \times 100 \quad (1)$$

where, ΔH_m is enthalpy of fusion at melting temperature T_m, ΔH_{cc} is the enthalpy of fusion at cold crystallization temperature $T_{cc,}$ and ΔH_{mp} is the heat of fusion of a perfect PLA crystal which is 93.6 J/g.[27]

X-ray Diffraction (XRD). XRD analysis of pure PLA and its bionanocomposite films was carried out under air atmosphere at room temperature on a Bruker A8 advance instrument using Cu-Kα ($\lambda = 0.15406$ nm) radiation operating at 40 kV and 40

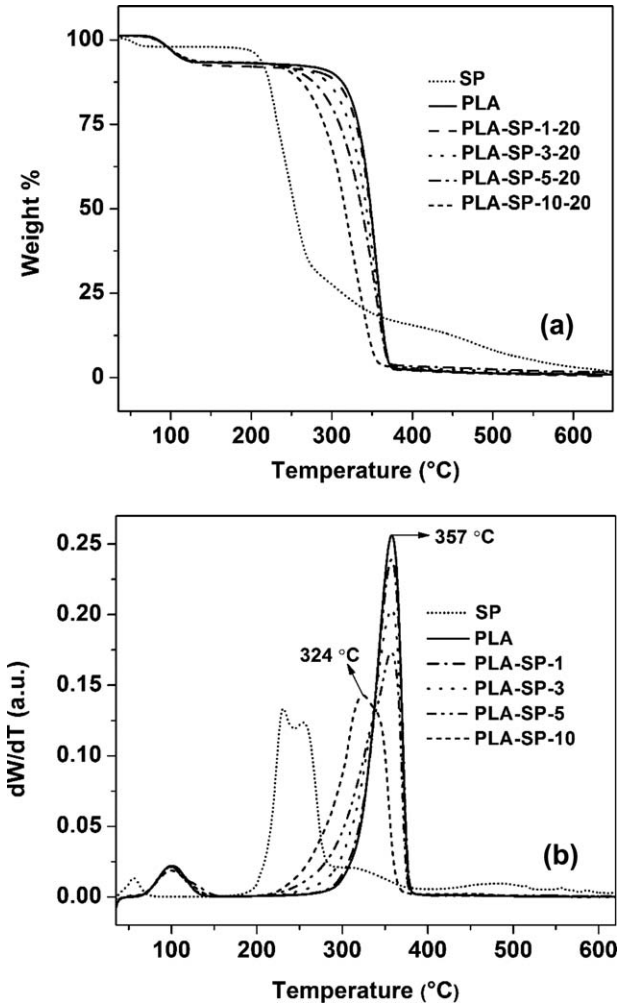

Figure 1. (a) TGA curves and (b) DTG curves for SP, PLA and PLA-SP composites at the heating rate of 20°C/min.

mA. The diffraction data were recorded in the 2θ range of 1–50° with a scanning rate of 0.05° s^{-1} and 0.5 s step size.

Fourier Transform Infrared Spectroscopy (FTIR). FT-IR spectra for pure PLA and composite films were recorded between 4000 and 450 cm^{-1} region using a Shimadzu IR affinity-1 model spectrometer operated under attenuated total reflectance (ATR) mode.

Transmission Electron Microscopy (TEM). The dispersion of SP in PLA matrix was visually observed using transmission electron microscopy (JEOLJEM 2100), operated at 200kV. By direct casting of polymer composite solution over the carbon-coated copper TEM grid, images of the bionanocomposite were obtained.

UV-Visible Spectrometry. Transparency measurements were carried out using a UV-Visible spectrophotometer (Make: Perkin Elmer, Model: Lambda 35). The wavelength range for the measurements was varied between 200 and 600 nm with a scan rate of 50 nm/min and a spectral bandwidth of 2 nm.

Mechanical Testing. The uni-axial tensile properties (modulus, tensile strength, elongation at break) were measured at room temperature with a 50 kN load cell on a tensile tester. The cross-head speed was set at 5 mm/min. specimens used in this method were prepared according to ASTM standard D 882-12. Three specimens of each sample were tested and the average results were reported.

Oxygen Permeability Measurements. The oxygen permeability of PLA and PLA-SP composites was measured using a PBI-Dansensor (Ringsted, Denmark) OPT 5000 oxygen permeability tester at 23 ± 0.03°C and 50 ± 2% RH. Dry nitrogen containing less than 0.1 ppm oxygen (Alphagaz 2, Air-Liquid Denmark, Ballerup, Denmark) was used as carrier gas and pure oxygen (purity: 99.995%), Air-Liquid Denmark) was used as a test gas. Inlet pressure was maintained at ~4 Kg/cm^2. At least three replicate tests were performed for each sample films.

RESULTS AND DISCUSSION

Thermogravimetric Analysis

Thermo graph shown in Figure 1(a) indicates the weight loss profile in two stages: first stage of weight loss ~100°C is due to evaporation of adsorbed moisture. The second stage of thermal degradation process of PLA that occurs in the temperature regime of 300–375°C can be mainly due to intra-molecular trans-esterification (backbitting reaction).[27,38–42] From the TGA profiles, the onset of degradation (T_{onset}) that corresponds to 10 wt % loss is determined by extrapolating the peak of degradation of the samples. Similar to neat PLA, PLA-SP composites also exhibit two stages of degradation. When 10% weight loss is taken as a point of comparison, T_{onset} of the composites for PLA is 301°C and declines to 288°C for 1 wt % of SP content. As the SP content increases from 3 to 10 wt %, T_{onset} reduces from 278 to 249°C. The possible reason is the contribution of thermal decomposition profile of SP. It can be observed from the TGA curves that SP is thermally stable up to 180°C. Hence, with increasing the concentration of SP content in the PLA matrix, sucrose content also increases in turn leading to early onset degradation of PLA composites.

However, thermal decomposition of SP occurs via three stages. First stage of thermal degradation is due to the adsorbed moisture. The second region of weight loss observed from 180 to 240°C reflects splitting of glycosidic bridge between glucose and fructose groups present in the sucrose.[43,44] The third region of weight loss of SP observed at 240°C corresponds to the decomposition of ester groups present in the palmitate tail.[45,46]

The decomposition temperatures at 50% weight loss for neat PLA, 1, 3, 5, and 10 wt % PLA-SP composites are 348, 347, 336, and 316°C, respectively. The temperature of 50% weight loss of PLA is comparable with PLA composites (SP: 1 and 3 wt %). In rest of the composites, a considerable difference in weight loss can be seen. This is because of the excess water released during sucrose hydrolysis that induces autocatalytic cleavage of ester groups.[47,48] Another important thermal property is the temperature corresponding to the maximum rate of weight loss (T_{max}), which is defined as the peak value of the first derivative of the TGA curve. The first derivative curves for SP, neat PLA, and PLA-SP composites are depicted in Figure 1(b). All the samples (neat PLA and PLA composites)

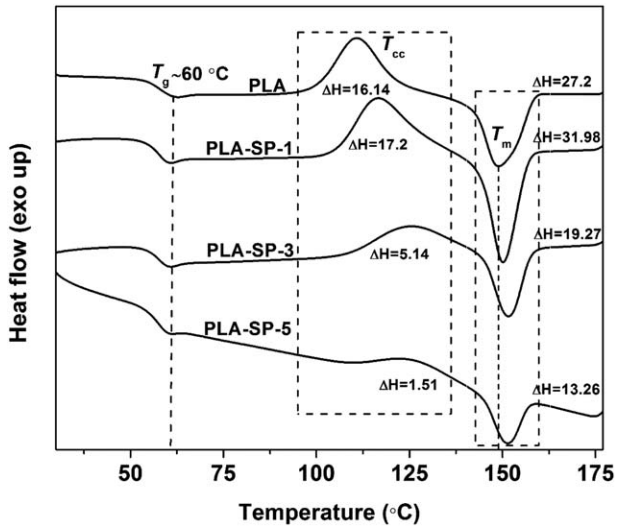

Figure 2. DSC heating curves for PLA, and PLA-SP composites at the heating rate of 5°C/min.

demonstrate single peak in the DTG curves indicating that the main degradation of these materials proceed in one step. It can be noticed that there is no change in the T_{max} value (357°C) for neat PLA and its composites (up to 5 wt % of SP loading). In the case of 10 wt % of SP reinforcement in the PLA matrix, T_{max} shifts to lower temperature (324°C). The downturn exhibited is probably due to the increased acidic sites created during the degradation of higher loadings of SP in the PLA matrix.[49,50] Moreover, it can be observed from Figure 1(a,b), the thermal stability of PLA-SP-10 is drastically reduced in comparison to PLA-SP-5. Hence, PLA-SP-5 is considered as optimum loading and further characterizations are carried out only up to 5 wt % SP loading.

Differential Scanning Calorimetry

DSC analysis is carried out to evaluate crystallization and melting behaviors of PLA and PLA-SP composites. DSC second heating thermographs of neat PLA and PLA bionanocomposites are shown in Figure 2. In this study, the influence of addition of nano bio-filler (SP) on the crystalline morphology of PLA is slightly positive effect which can be seen from Table I. The melting region of PLA provides unimodal endothermic peak, ($T_m = 149$°C), which indicates the presence of PLA in α-crystalline form.[51–54] Incorporation of the bio-filler does not result in bimodal endothermic melting peaks for PLA bionanocomposites (Figure 2). Unimodal endotherms reveal the melting of stable crystals of PLA formed due to the absence of heterogeneous distribution of the crystals as well as uniform crystal thickness developed in PLA after reinforcement of the SP filler.[55] Addition of bio-filler in PLA matrix shifts T_m to slightly higher value. The shift in T_m indicates that the addition of the SP filler do not lower the molecular weight of PLA. The current result specifies that the SP acts as a better nucleating agent by enhancing the T_m, in contrast to the recently reported reinforcements such as organically modified montmorillonite (MMT-TAC),[17] nickel-containing layered double hydroxides (LDH),[56] nanoclay,[57] and talc[34] used for developing PLA composites. The decrease in the T_m values of about ~6, 8, 1, and 3°C, is reported for the respective fillers in comparison to neat PLA. The reduction in the heat of fusion for melting peaks is observed when the SP content increases. This phenomenon is attributed to the strong hydrogen bonding interaction between SP and PLA.[58]

Several studies reported that lower values of T_g for PLA composites could be attributed to the presence of short chain molecules due to filler induced PLA degradation and reduced macromolecular interactions.[52,59] Interestingly, in this study, T_g (61°C) remains unaltered for the PLA composites indicating that the reinforcement of SP does not induce the formation of short chain PLA molecules. Because nanocomposite films are prepared by solution casting techniques at room temperature instead of melt extrusion where degradation generally occurs if the material is exposed for longer time. It can be seen from the DSC curves that in comparison with neat PLA, the cold crystallization temperature (T_{cc}) increases significantly by 6, 14, 14°C for 1, 3, 5 wt % loading of SP, respectively. The increase in T_{cc} is due to the fact that the addition of SP suppresses the diffusion rate leading to the slower migration of the polymer chains to the surface of the nucleus.[60,61] The higher T_{cc} values with broadening of its peak width obtained for the composites signify that the crystallization rate becomes slower than that of neat PLA; both homogeneous and heterogeneous crystallization take place within the composites.[60] The increase in T_{cc} could be further considered due to the nucleation effect of SP incorporated in the PLA matrix.[62] Another reason for enhancement in the crystallization temperature for the PLA composites may be the formation of ordered α-form of PLA crystals during cold crystallization process.[63]

DSC analysis of nanocomposite films provides data on ΔH_{cc} and ΔH_m, from which useful insight into interactions between PLA and SP can be inferred.[64] It is noticed from Table I, that ΔH_{cc} and ΔH_m for PLA-SP-1 are slightly higher in comparison with neat PLA. This is indicative of stable crystals of PLA formed during crystallization process and hence, slight

Table I. DSC Results for PLA and PLA-SP Composites

S.No	Sample	T_g (°C)	T_c (°C)	T_m (°C)	ΔH_c	ΔH_m	% X_c
1	PLA	61	110	149	16.14	27.20	~12
2	PLA-SP-1	60	117	150	17.20	31.98	~16
3	PLA-SP-3	60	125	152	5.14	19.27	~15
4	PLA-SP-5	60	125	152	1.51	13.16	~12

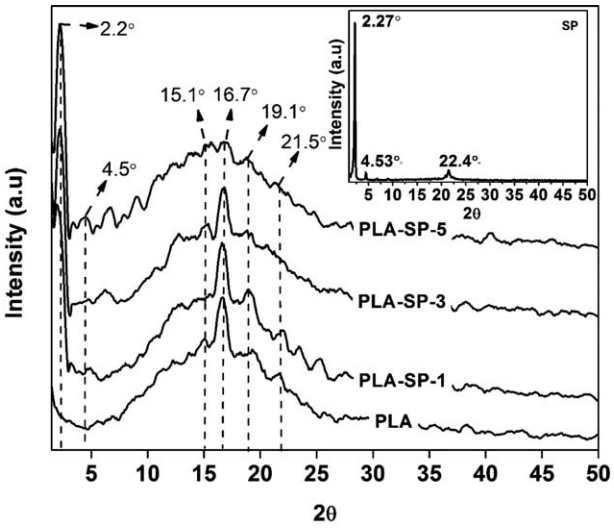

Figure 3. XRD patterns for SP, PLA, and PLA-SP composites.

enhancement in the percentage crystallinity is observed for 1 wt % SP incorporation. In contrast, ΔH_{cc} and ΔH_m gradually decreases with further increase in the SP content, which is due to the melting of PLA crystallites.[65] Due to this fact, at higher loadings, despite of enhancement in crystallization temperature, crystallization peaks broaden leading to decrease in % crystallinity when compared with 1 wt % loading of SP. DSC results reveal that there is a slight improvement in the crystallinity of the PLA at very low concentration of SP.

XRD Analysis

XRD analysis as shown in Figure 3 was performed to understand the addition of SP on the crystalline structure of PLA. The crystal structure of PLA has been the topic of extensive studies. In general, depending on the preparation conditions, two crystal structures may be obtained for PLA: a pseudoorthorhombic α-structure with left handed 10_3 helices chain conformation and a less stable β-orthorhombic structure with 3_1 chain conformation.[66] The structural analysis of neat PLA displays the most intense peak at $2\theta = 16.7°$ corresponding to the reflections from (110) and/or (200) planes of orthorhombic α-crystalline phase. The less intense peaks appeared at $2\theta = 15.1$, 19.1, and 21.5° are from the (010), (203), and (210) planes of α-phase, respectively.[61,67] The PLA diffraction pattern presented herein matches closely with the α-crystalline structure. XRD analysis of SP shows a sharp intense crystalline peak at $2\theta = 2.27°$, corresponding to the palmitate ester tail present in the bio-filler. The less intense diffraction peaks at 4.53 and 22.4° are attributed to the head group of SP.[45]

The nanocomposite diffraction intensities are vertically offset for clarity of presentation. The peak at $2\theta = 4.53°$ corresponding to the head group of SP is not identified at low SP content, due to their relatively low concentration of SP in the PLA composites. The intensity of the crystalline peak corresponding to the palmitate ester group increases with an increase in SP concentration. This increased intensity is due to the more diffracted X-rays from the dispersion of the additional reinforcing agent in the PLA matrix.[66] For all the bionanocomposites, the peak position ($2\theta = 16.7°$) corresponding to the crystal structure of PLA is not altered. It is clear that lattice parameters are not altered by the addition of SP.[68–70] The reflection representing the crystal structure of PLA is present in all the bio-nanocomposite indicating that the incorporation of SP has not significantly disrupted the crystal structure within the PLA matrix.[68–70] However, it can be seen from Figure 3 that the intensity of the peak ($2\theta = 16.7°$) corresponding to the crystal structure of PLA increases for the PLA-SP-1 sample. This

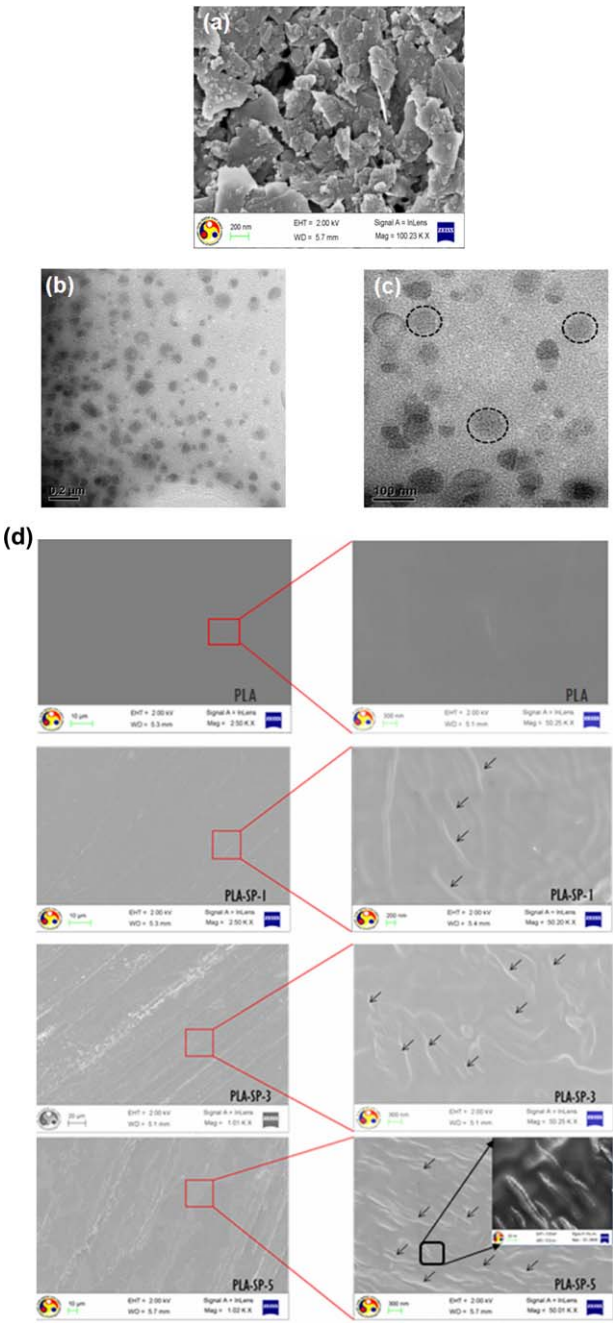

Figure 4. (a) FE-SEM image for SP, (b) and (c) TEM micrographs for PLA-SP-1 at different magnifications, (d) FE-SEM images for PLA and PLA-SP bionanocomposites. [Color figure can be viewed in the online issue, which is available at wileyonlinelibrary.com.]

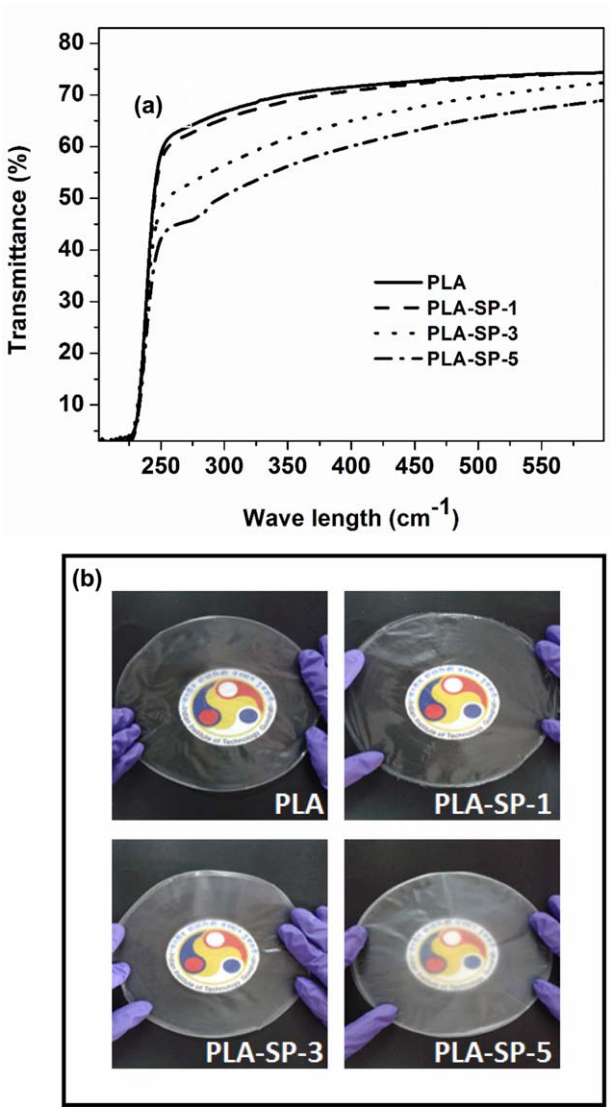

Figure 5. (a) % Transparency measurements and (b) contact transparency images for PLA and PLA-SP composites. [Color figure can be viewed in the online issue, which is available at wileyonlinelibrary.com.]

supports the increase in amount of crystallinity[66] as discussed in DSC analysis. The presence of a shoulder at around $2\theta = 19.1°$ for PLA-SP bionanocomposite elucidates that SP has the ability to act as a nucleating agent, by increasing the crystallinity of the composite system.[71]

Morphology of PLA Bionanocomposite Films

The morphological feature of SP is examined by FE-SEM as depicted in Figure 4(a). The images reveal that the SP exhibits a plate-like structure. The dispersed SP platelets (1 wt %) within PLA matrix can also be seen from TEM micrographs in Figure 4(b,c). The average particle size of the reinforced SP in the PLA matrix is found to be 50.84 ± 11.98 nm. In the TEM micrograph, the sheet-like particles (dark portion indicated in circles) represent the bio-filler SP and the bright areas represent the PLA matrix. The appearance of homogeneously dispersed SP in the composite system is visualized from the TEM image. The uniform dispersion of SP in the PLA matrix can also be observed from the FE-SEM images for PLA and PLA-SP bionanocomposites shown in Figure 4(d). It is indicative from the FE-SEM image (inset) pictoriated at higher magnification for PLA-SP-5 bionanocomposites that plate like structure of SP filler is homogenously dispersed in the PLA matrix without agglomeration.

Transparency

From Figure 5(a), it can be observed that, 63% (at 250 nm) and 66% (at 300 nm) of UV light are transmitted in the neat PLA film respectively. This indicates that most of the UV-B radiation (315–280 nm) passes through PLA film.[72,73] In case of PLA-SP-5 bionanocomposite film, the reduction in the UV-B transmittance of 32%, 30% at 250, 300 nm, respectively, is noticed in comparison to neat PLA. At 575 nm, the visible light transmittance for neat PLA, and PLA-SP-5 films is observed to be 72 and 63%, respectively which is 12.5% reduction in transmittance when compared with neat PLA. This is an advantage provided by SP filler, such that the optical clarity remains very close to that of the neat PLA film, with only a slight decrease in transparency with increase in SP wt % loadings. The contact transparency images for PLA and PLA-SP composites are also illustrated in Figure 5(b). As observed, all the PLA-composite films illustrate almost a similar contact transparency in comparison with neat PLA. This observation seems to indicate that there exists a better compatibility between the filler and PLA matrix.[23]

Fourier Transform Infrared Spectroscopy

Figure 6 depicts the FTIR spectra of SP, PLA, PLA-SP composites. In the case of PLA, a band observed around 3500 cm^{-1} corresponds to the stretching of hydroxyl groups present as end group in PLA backbone.[57] The strong bands at 3000 and 2937 cm^{-1} correspond to the asymmetric and symmetric mode of C-H stretching, respectively. An absorption band present in the region of 1700–1800 cm^{-1} is attributed to the carbonyl group present in the ester linkage of the PLA matrix.[74] The existence of CH_3 band in the PLA is characterized by the presence of peak at 1456 cm^{-1}. The appearance of band at

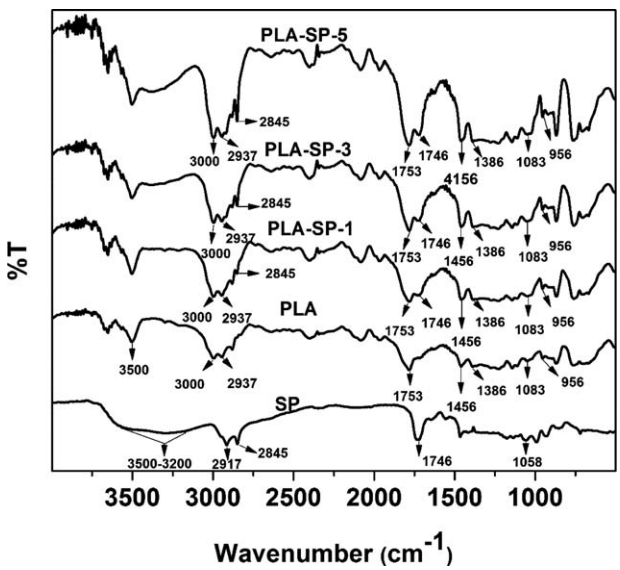

Figure 6. FTIR spectra for SP, PLA, and PLA-SP composites.

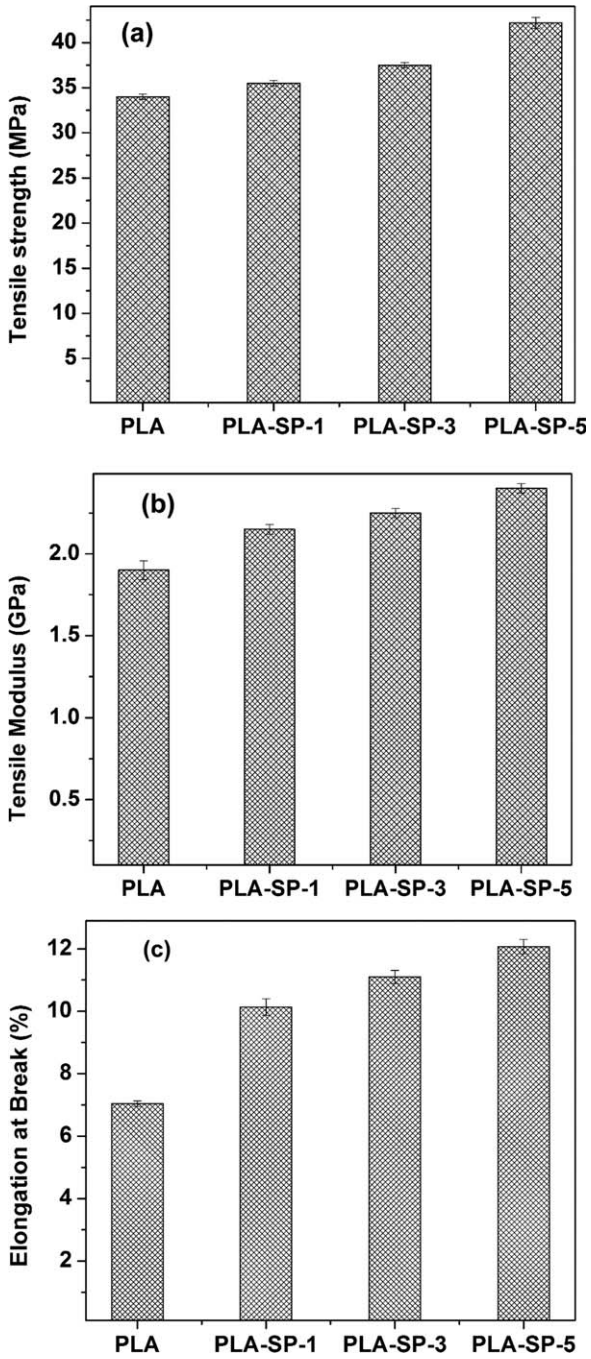

Figure 7. (a) Tensile strength, (b) modulus, and (c) elongation at break for PLA and PLA-SP composites.

1386 cm^{-1} is assigned to the C-H deformation.[74] The band present around 1083 cm^{-1} is due to the C-O asymmetric group of ester groups.[75] The stretching frequency observed at 956 and 922 cm^{-1} is mainly attributed to the rocking mode of CH_3.[57,74,75] In the FTIR spectrum of SP, the strong absorption band found in the region of 3500–3200 cm^{-1} characterizes the O-H stretching of the free hydroxyl groups of SP. The stretching bands at 2917 and 2845 cm^{-1} are assigned to the methylene and terminal methyl groups of palmitate chain of SP, respectively. The band at 1058 cm^{-1} corresponds to the C-O-C stretching vibration of SP.[44,55]

It can be observed from the FTIR spectrum of PLA-SP bionanocomposites that the hydroxyl region is exhibited in the range of 3600–3200 cm^{-1} upon addition of SP in the PLA matrix.[76,77] When the carbonyl region (1700–1800 cm^{-1}) of PLA and PLA-SP composites are closely visualized, the corresponding peak become broadened and split into two small peaks (1753 and 1746 cm^{-1}) for PLA-SP composites. This reveals the existence of intermolecular interaction between PLA and SP.[76,77] As the SP loading increases in the PLA matrix, the content of methylene and terminal methyl groups of palmitate in the PLA composites also increases. This fact is well revealed by the increase in the intensity of the bands (2845 cm^{-1}) corresponding to terminal methyl groups of palmitate chain of SP.[76,77] The increase in sharpness preceded by the decrease in broadness of the corresponding band region (3200–2800 cm^{-1}) in comparison with pure PLA also supports the above statement.

Mechanical Properties

Figure 7 shows the effect of SP content on the mechanical properties of PLA matrix. It can be seen from Figure 7(a) that the tensile strength of PLA composites increases with an increase in the SP content. The PLA-SP-5 composite demonstrates a maximum tensile strength and modulus of 41 MPa, 2.2 GPa, respectively over neat PLA (tensile strength of 34 MPa and modulus of 2 GPa). The addition of SP improves the tensile strength, which is an indication of good adhesion between PLA and the filler. The obtained results are consistent with results reported by Graupner[76] for PLA-cotton fiber composites. As can be seen from Figure 7(b), the incorporation of SP in the PLA matrix enhances the tensile modulus for PLA composites, indicating the reinforcing action of the filler. In comparison with neat PLA, the increased modulus of PLA-SP composites compared with PLA matrix can also be associated with the restrictions of molecular mobility and deformability imposed by the presence of SP. Figure 7(c) shows the elongation at break of PLA and PLA-SP composites. The value obtained at 5 wt % of SP content is 56% higher than that of neat PLA. It implies that the ductility of PLA is effectively improved by the incorporation of SP. This behavior is due to the plasticization effect provided by hydrophobic moieties of SP reinforced in the PLA matrix. The results also indicate that SP acts as a bridge to prolong the fracture process of PLA composites and thereby reduces the sudden risk of failure. Enhancement in the elongation at break values obtained in this study is comparable to the PLA-chicken feather fiber composites (~55%) reported by Cheng et al.[77] However, drop in the tensile strength and elongation at break (%) is also reported for PLA-starch[28] and PLA-soy protein.[35] It is discussed that both the tensile strength and elongation at break (%) of these composites decreases due to the lack of affinity between filler and PLA.[28,35]

Film Permeability

One of the main functions of the films for food packaging is to decrease the oxygen transmission between the food and the surrounding atmosphere. Hence, oxygen permeability (OP) becomes a significant physical parameter to be considered. In a view to know the effect of novel filler "SP" in terms of barrier properties, oxygen permeation studies are carried out beyond 5 wt % SP loading (i.e., 15 and 30 wt % SP). Figure 8 shows the

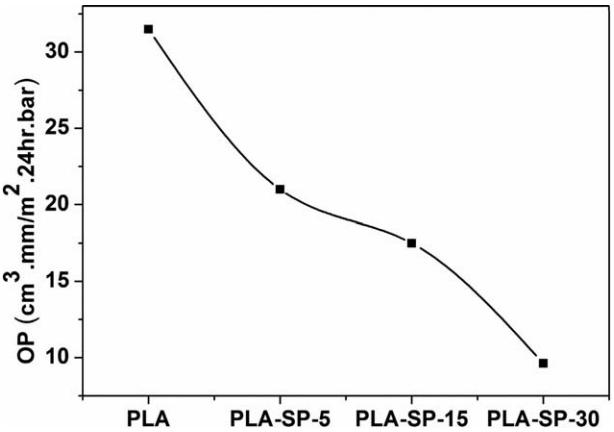

Figure 8. Oxygen permeability measurements for PLA and PLA-SP composites.

OP values of PLA and PLA bionanocomposites reinforced with SP. Bionanocomposites display reduction in the OP values with respect to PLA film and the OP values reduces drastically when the SP content increases. This underlines the positive effect of SP in increasing the barrier properties of PLA. The best positive influence is confirmed for the PLA-SP-30 bionanocomposite films where the reduction in OP by ~69.46% is noticed in comparison to PLA (Figure 8). It is well known that the transport properties of gases through PLA films are strongly influenced by tortuousity of their path, which is dependent on several factors including shape and aspect ratio of the filler, degree of exfoliation or dispersion, filler loading and orientation, adhesion to the matrix, moisture activity, filler-induced crystallinity, polymer chain immobilization, filler-induced solvent retention and porosity.[78] In our case, dispersion of SP to a higher extent in the PLA matrix as shown in TEM analysis and good adhesion between SP with PLA matrix via intra molecular hydrogen bonding as revealed in FTIR analysis results in a more efficient barrier effect. The reduction in OP of 15.95 and 7.97% are reported for butylated hydroxytoluene (BHT)/poly(ethylene glycol) (PEG 400) and α-tocopherol/BHT/PEG 400 blended PLA films,[79] respectively. Around 47–62% reduction of OP for PLA/closite-B composite is also reported in a previous study.[80] However, for food packaging applications, consideration of compatibility of filler with food during storage becomes a prerequisite factor. In comparison to the literature data,[79,80] a significant enhancement in the oxygen barrier effects for PLA-SP bionanocomposites is evidenced and also the filler chosen in the current work is a food additive which has definite compatibility with food during storage. Highly dispersed state of SP in the PLA matrix increases the distance (tortuous path) that the oxygen molecules have to travel through the PLA matrix and the same is reflected in terms of barrier effects. High oxygen barrier effects and transparent nature of the films induced by food additive SP promises that PLA-SP bionanocomposite films can be used as potential materials for food packaging applications.

CONCLUSION

The incorporation of SP has brought considerable improvements in the thermal, mechanical, and barrier properties of PLA. The DTG thermographs reveal that incorporation of SP decelerates the thermal degradation rate of PLA composites. From the DSC analysis, it is observed that crystallization takes place in PLA through homogeneous crystallization. PLA-SP bionanocomposites exhibited both homogeneous as well as heterogeneous crystallization which confirms the nucleation effect of SP. The higher T_c values obtained for the composites indicate that crystallization rate become dependent on filler loading. Uniform dispersion of SP in the PLA matrix perceived in the morphological analyses showed profound impact on the mechanical and barrier properties. In terms of mechanical properties, SP indeed improves the elongation at break (%) due to its plasticizing property. The best positive effect is observed for PLA-SP composites, where the reduction in OP by 69.46% is noticed in comparison with neat PLA. This effect in terms of barrier properties is due to increase in the tortuous path, which can be correlated to the uniform dispersion of SP in the PLA matrix evidenced in morphological studies.

ACKNOWLEDGMENTS

The authors sincerely thank the Central Instrument Facility (CIF), Indian Institute of Technology Guwahati for providing FE-SEM and TEM facilities. The authors sincerely thank the Department of Chemicals and Petrochemicals, Ministry of Chemicals and Fertilizers, Government of India - funded Center of Excellence for Sustainable Polymers at IIT Guwahati for Research facilities to perform this research work. Authors also thank Dr. David Plackett, DTU, Denmark, for sharing biofillers and OTR facility, used in this study.

REFERENCES

1. Zhang, B.; Wang, Q. *J. Agric. Food Chem.* **2012**, *60*, 4162.
2. Ali, S. S.; Tang, X.; Alavi, S.; Faubion, J. *J. Agric. Food Chem.* **2011**, *59*, 12384.
3. Simoneit, B. R. T.; Medeiros, P. M.; Didyk, B. M. *Environ. Sci. Technol.* **2005**, *39*, 6961.
4. Goffin, A. L.; Raquez, J. M.; Duquesne, E.; Siqueria, G.; Habibi, Y.; Dufresne, A.; Dubois, P. *Biomacromolecules* **2011**, *12*, 2456.
5. Ray, S. S.; Bousmina, M. *Prog. Mater. Sci.* **2005**, *50*, 962.
6. Magniez, K.; Voda, A. S.; Kafi, A. A.; Fichini, A.; Guo, Q.; Fox, B. L. *ACS Appl. Mater. Interfaces* **2013**, *5*, 276.
7. Oksman, K.; Skrifvars, M.; Selin, J. F. *Compos. Sci. Technol.* **2003**, *63*, 1317.
8. Jain, R. A. *Biomaterials* **2000**, *21*, 2475.
9. Mikos, A. G.; Lyman, M. D.; Freed, L. E; Langer, R. *Biomaterials* **1994**, *15*, 55.
10. Park, T. G.; Cohen, S.; Langer, R. *Macromolecules* **1992**, *25*, 116.
11. Liu, H.; Song, W.; Chen, F.; Guo, L.; Zhang, J. *Macromolecules* **2011**, *44*, 1513.
12. Hoglund, A.; Hakkarainen, M.; Albertsson, A. C. *Biomacromolecules* **2010**, *11*, 277.
13. Ljungberg, N.; Wesslen, B. *Biomacromolecules* **2005**, *6*, 1789.

14. Ray, S. S. *Acc. Chem. Res.* **2012**, *45*, 1710.
15. Bordes, P.; Pollet, E.; Averous, L. *Prog. Polym. Sci.* **2009**, *34*, 125.
16. Ray, S. S.; Okamoto, M. *Prog. Polym. Sci.* **2003**, *28*, 1539.
17. Wang, D. Y.; Gohs, U.; Kang, N. J.; Leuteritz, A.; Boldt, R.; Wagenknecht, U.; Heinrich, G. *Langmuir* **2012**, *28*, 12601.
18. Li, Yonghui.; Sun, X. S. *Biomacromolecules* **2010**, *11*, 1847.
19. Svagan, A. J.; Akesson, A.; Cardenas, M.; Bulut, S.; Knudsen, J. C.; Risbo, J.; Plackett, D. *Biomacromolecules* **2012**, *13*, 397.
20. Ray, S. S.; Yamada, K.; Okamoto, M.; Ogami, A.; Ueda, K. *Chem. Mater.* **2003**, *15*, 1456.
21. Yan, S.; Yin, J.; Yang, J.; Chen, X. *Mater. Lett.* **2007**, *61*, 2683.
22. Park, S. H.; Lee, S. G; Kim, S. H. *Compos. A* **2013**, *46*, 11.
23. Sun, Y.; He, C. *ACS Macro Lett.* **2012**, *1*, 709.
24. Zhang, J.; Lou, J.; Ilias, S.; Krishnamachari, P.; Yan, J. *Polymer* **2008**, *49*, 2381.
25. Duncan, T. V. *J. Colloid. Interface Sci.* **2011**, *363*, 1.
26. Corma, A.; Iborra, S.; Velty, A. *Chem. Rev.* **2007**, *107*, 2411.
27. Garlotta, D. *J. Polym. Environ.* **2001**, *9*, 63.
28. Lu, D. R.; Xiao, C. M.; Xu, S. J. *Express Polym. Lett.* **2009**, *3*, 366.
29. Koutsomitopoulou, A. F.; Benezet, J. C.; Bergeret, A.; Papanicolaou, G. C. *Powder Technol.* **2014**, *255*, 10.
30. Fortunati, E.; Luzi, F.; Puglia, D.; Dominici, F.; Santulli, C.; Kenny, J. M.; Torre, L. *Eur. Polym. J.* **2014**, *56*, 77.
31. Bonilla, J.; Fortunati, E.; Vargas, M.; Chiralt, A.; Kenny, J. M. *J. Food Eng.* **2013**, *119*, 236.
32. Fortunati, E.; Peltzer, M.; Armentano, I.; Torre, L.; Jimenez, A.; Kenny, J. M. *Carbohydr. Polym.* **2012**, *90*, 948.
33. Lee, B. H.; Kin, H. S.; Lee, S.; Kim, H. Y.; Dorgan, J. R. *Compos. Sci. Technol.* **2009**, *69*, 2573.
34. Battegazzore, D.; Bocchini, S.; Frache, A. *Express Polym Lett.* **2011**, *5*, 849.
35. Zhu, R.; Liu, H.; Zhang, J. *Ind. Eng. Chem. Res.* **2012**, *51*, 7786.
36. Goriparthi, B. K.; Suman, K. N. S.; Rao, N. M. *Compos. A* **2012**, *43*, 1800.
37. Wang, Y.; Xu, Y.; He, D.; Yao, W.; Liu, C.; Shen, C. *Mater. Lett.* **2014**, *128*, 85.
38. Fan, Y.; Nishida, H.; Shirai, Y.; Endo, T. *Polym. Degrad. Stabil.* **2004**, *84*, 143.
39. Taubner, V.; Shishoo, R. *J. Appl. Polym. Sci.* **2001**, *79*, 2128.
40. Wang, Y.; Mano, J. F. *Eur. Polym. J.* **2005**, *41*, 2335.
41. Wang, Y.; Steinhoff, B.; Brinkmann, C. Alig, I. *Polymer* **2008**, *49*, 1257.
42. Yu, H.; Huang, N.; Wang, C.; Tang, Z. *J. Appl. Polym. Sci.* **2003**, *88*, 2557.
43. Hosseini, S. G.; Pourmortazavi, S. M.; Hajimirsadeghi, S. S. *Comb. Flame* **2005**, *141*, 322.
44. Predoi, D. *J. Nanomater. Biosci.* **2010**, *5*, 373.
45. Fang, G.; Li, H.; Chen, Z.; Liu, X. *Sol. Energy Mater. Sol. Cells* **2011**, *95*, 1875.
46. Li, Y.; Wang, S.; Yang, X.; Zhang, X. *Int. J. Nanosci.* **2009**, *8*, 97.
47. Antheunis, H.; Meer, J. C. V. D.; Geus, M. D.; Heise, A.; Koning, C. E. *Biomacromolecules* **2010**, *11*, 1118.
48. Janorkar, A. V.; Metters, A. T.; Hirt, D. E. *Macromolecules* **2004**, *37*, 9151.
49. Kelly, F. H. C.; Brown, D. W. *Sugar Technol. Rev.* **1978**, *6*, 1.
50. Richards, G.N. *Int. Sugar J.* **1986**, *88*, 145.
51. Valapa, R.; Pugazhenthi, G.; Katiyar, V. *Int. J. Biol. Macromol.* **2014**, *65*, 275.
52. Peng, F.; Shaw, M. T.; Olson, J. R.; Wei, M. *J. Phys. Chem. C* **2011**, *115*, 15743.
53. Sawai, D.; Takahashi, K.; Sasashige, A.; Kanamoto, T.; Hyon, S. H. *Macromolecules* **2003**, *36*, 3601.
54. Hoogsteen, W.; Postema, A. R.; Pennings, A. J.; Brinke, G. T. *Macromolecules* **1990**, *23*, 634.
55. Bharadwaj, R.; Mohanty, A. K.; Drzal, L. T.; Pourboghrat, F.; Misra, M. *Biomacromolecules* **2006**, *7*, 2044.
56. Shan, X.; Song, L.; Xing, W.; Hu, Y.; Lo, S. *Ind. Eng. Chem. Res.* **2012**, *51*, 13037.
57. Vasanthan, N.; Ly, H.; Ghosh, S. *J. Phys. Chem. B* **2011**, *115*, 9556.
58. Ali, S. S.; Tang, X.; Alavi, S.; Faubion, J. *J. Agric. Food Chem.* **2011**, *59*, 12384.
59. Liu, L.; Jin, T. Z.; Coffin, D. R.; Hicks, K. B. *J. Agric. Food Chem.* **2009**, *57*, 8392.
60. Katiyar, V.; Gerds, N.; Koch, C. B.; Risbo, J.; Hansen, H. C. B.; Plackett, D. *Polym. Degrad. Stabil.* **2010**, *95*, 2563.
61. Zhang, K.; Mohanty, A. K.; Misra, M. *ACS Appl. Mater. Interfaces* **2012**, *4*, 3091.
62. Goffin, A. L.; Raquez, J. M.; Duquesne, E.; Siqueria, G.; Habibi, Y.; Dufresne, A. *Biomacromolecules* **2011**, *12*, 2456.
63. Pan, P.; Yang, J.; Shan, G.; Bao, Y.; Weng, Z.; Cao, A.; Yazawa, K.; Inoue, Y. *Macromolecules* **2012**, *45*, 189.
64. Ali, S. S.; Tang, X.; Alavi, S.; Faubion, J. *J. Agric. Food Chem.* **2011**, *59*, 12384.
65. Zeng, J. B.; Li, Y. D.; He, Y. S.; Wang, Y. Z. *Ind. Eng. Chem. Res.* **2011**, *50*, 6124.
66. Krikorian, V.; Pochan, D. J. *Chem. Mater.* **2003**, *15*, 4317.
67. Barrau, S.; Vanmansart, C.; Moreau, M.; Addad, A.; Stoclet, G.; Lefebvre, J. M.; Seguela, R. *Macromolecules* **2011**, *44*, 6496.
68. Desantis, P.; Kovacs, A. J. *Biopolymers* **1968**, *6*, 299.
69. Brizzolara, D.; Cantow, H. J.; Diederichs, K.; Keller, E.; Domb, A. J. *Macromolecules* **1996**, *29*, 191.
70. Hoogsteen, W.; Postema, A. R.; Pennings, A. J.; Tenbrinke, G.; Zugenmaier, P. *Macromolecules* **1990**, *23*, 634.
71. Fortunati, E.; Peltzer, M.; Armentano, I.; Torre, L.; Jimenez, A.; Kenny, J. M. *Carbohydr. Polym.* **2012**, *90*, 948.
72. Auras, R.; Harte, B.; Selke, S. *Macromol. Biosci.* **2004**, *4*, 835.

73. Hernandez, J. J.; Garcia-Gutierrez, M. C.; Nogales, A.; Rueda, D. R.; Kwiatkowska, M.; Szymczyk, A.; Roslaneic, Z.; Concheso, A.; Guinea, I.; Ezquerra, T. A. *Compos. Sci. Technol.* **2009**, *69*, 1867.

74. Pamula, E.; Blazewicz, M.; Paluszkiewicz, C.; Dobrzynski, P. *J. Mol. Struct.* **2001**, *596*, 69.

75. Mai, T. T. T.; Nguyen, T. T. T.; Le, Q. D.; Park, J. S. *Adv. Nat. Sci. Nanosci. Nanotechnol.* **2012**, *3*, 25014.

76. Grapnuer, N. *J. Mater. Sci.* **2008**, *43*, 5222.

77. Cheng, S.; Lau, K.; Liu, T.; Zhao, Y.; Lam, P.; Yin, Y. *Compos. B* **2009**, *40*, 650.

78. Sanchez-Garcia, M. D.; Gimenez, E.; Lagaron, J. M. *Carbohydr. Polym.* **2008**, *71*, 235.

79. Byun, Y.; Kim, Y. T.; Whiteside, S. *J. Food Eng.* **2010**, *100*, 239.

80. Katiyar, V.; Gerds, N.; Koch, C. B.; Risbo, J.; Hansen, H. S. B.; Plackett, D. *J. Appl. Polym. Sci.* **2011**, *122*, 112.